Laurdan Solvatochromism: Solvent Dielectric Relaxation and Intramolecular Excited-State Reaction

Mathias Viard,* Jacques Gallay,# Michel Vincent,# Olivier Meyer,* Bruno Robert,§ and Maïté Paternostre*
*Equipe "Physicochimie des systèmes polyphasés," URA CNRS 1218, Université Paris XI, FR-92296 Châtenay Malabry; #L.U.R.E., Université Paris XI, FR-91 Orsay; and §Section de Biophysique des protéines et des membranes, DBCM/CEA et URA CNRS 2096, FR-91191 Gif/Yvette, France

ABSTRACT Absorption, steady-state, and time-resolved fluorescence measurements have been performed on laurdan dissolved either in white viscous apolar solvents or in ethanol as a function of temperature. The heterogeneity of the absorption spectra in white oils or in ethanol is consistent with semiempirical calculations performed previously on Prodan. From steady-state and time-resolved fluorescence measurements in apolar media, an excited state reaction is evidenced. The bimodal lifetime distribution determined from the maximum entropy method (MEM) analysis is attributed to the radiative deexcitation of a "locally excited" (LE) state and of a "charge transfer" (CT) state, whereas a very short component (20 ps), the sign and the amplitude of which depend on the emission wavelength, is attributed to the kinetics of the interconvertion reaction. The observation of an isoemissive point in the temperature range from −50°C to −110°C in ethanol suggests an interconvertion between two average excited-state populations: unrelaxed and solvent-relaxed CT states. A further decrease in temperature (−190°C), leading to frozen ethanol, induces an additional and important blue shift. This low temperature spectrum is partly attributed to the radiative deexcitation of the LE state. Time-resolved emission spectra (TRES) measurements at −80°C in the ethanol liquid phase show a large spectral shift of ~2500 cm^{-1} (stabilization energy of the excited state: 7.1 $kcal \cdot M^{-1}$). The time-dependent fluorescence shift (TDFS) is described for its major part by a nanosecond time constant. The initial part of the spectral shift reveals, however, a subnanosecond process that can be due to fast internal solvent reorientation and/or to intramolecular excited-state reactions. These two relaxation times are also detected in the analysis of the fluorescence decays in the middle range of emission energy. The activation energy of the longest process is ~3 $kcal \cdot M^{-1}$. At −190°C, one subnanosecond and one nanosecond excited-state reactions are also evidenced. They are likely due to intramolecular rearrangements after the excitation, leading to the CT state and not to solvent relaxation, which is severely hindered in these temperature conditions. Therefore, both intramolecular and solvent relaxations are responsible for the large Stokes shift displayed by this probe as a function of solvent polarity. A possible scheme is proposed for the deexcitation pathway, taking into account the kinetics observed in these different solvents.

INTRODUCTION

Laurdan has been extensively used to study lipid organization in membranes, i.e., to follow the lipidic gel to liquid-crystalline phase transition (Parasassi et al., 1986, 1991), allowing notably the detection and the quantitation of coexisting domains (Parasassi et al., 1990). In particular, it has been shown to be an interesting tool for monitoring the effect of different membrane constituents, such as cholesterol, on the physical properties of the lipidic bilayer (Parasassi et al., 1994a,b). Recently laurdan has been used to study the vesicle-to-micelle transition of phospholipid-amphiphile systems (Heerklotz et al., 1994a,b; Paternostre et al., 1995). The evolution of the amphiphile partitioning between water and mixed lipid-amphiphile aggregates could be followed through laurdan fluorescence.

Because of its chemical structure (Fig. 1 *B*) (aliphatic tail of 12 carbons), laurdan is anchored in the membrane, with its fluorescent moiety exposed to the aqueous medium near the lipid polar headgroups. The extreme sensitivity of laurdan to lipid packing, which results in substantial red shifts of the emission spectrum, particularly when the membrane undergoes a gel-to-liquid crystalline phase transition, has been attributed to the high dipole moment of the molecule in its excited state. This dipole moment has been estimated to be between 20 D (Weber and Farris, 1979) and 8 D (Balter et al., 1988), depending on the authors. As a consequence, the dielectric relaxation process of the solvent molecules is generally supposed to govern the evolution of the fluorescence of laurdan, i.e., dielectric relaxation of the accessible water molecules at the membrane interface, with the accessibility and mobility of the water molecules depending on the lipid headgroups packing. Intramolecular relaxation processes, however, are also likely to occur, especially the rotation of the dimethylamino substituent, as in similar molecules (Soujanya et al., 1996). To correctly interpret the changes in the spectra of this probe located in various systems, a precise understanding of the fluorescence emission mechanisms is necessary.

Prodan, which is the prolyl derivative instead of the lauryl derivative for laurdan (Fig. 1, *A* and *B*), has been the subject of theoretical studies (Nowak et al., 1986; Ilich and Prendergast, 1989) aimed at identifying the highly polar electronic state responsible for its high spectroscopic sensitivity.

Received for publication 17 March 1997 and in final form 3 July 1997.
Address reprint requests to Dr. Maïté Paternostre, Equipe "Physicochimie des systèmes polyphasés," URA CNRS 1218, Université Paris XI, 5 Rue J.B. Clément, FR-92296 Châtenay-Malabry Cedex, France. Tel.: 33-1-4683-5644; Fax: 33-1-4683-5312; E-mail: paternos@cep.u-psud.fr.
© 1997 by the Biophysical Society
0006-3495/97/10/2221/14 $2.00

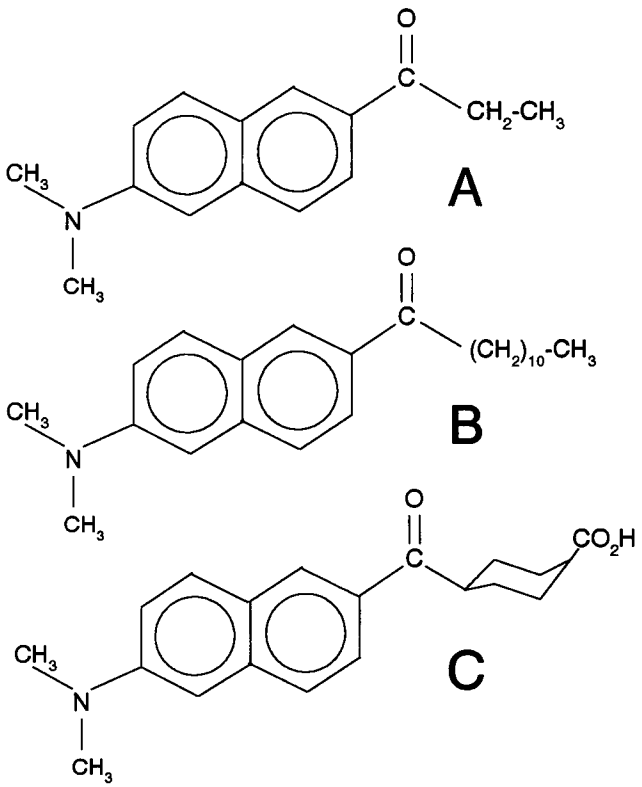

FIGURE 1 Chemical structures of Prodan (*A*), laurdan (*B*), and DANCA (*C*).

The results obtained in this respect showed that, according to x-ray diffraction data, the ground state is planar. Because this conformation could not lead to a highly polar state, the authors investigated the possibility that the high polar excited state of Prodan might result from a twisted intramolecular charge transfer (TICT) arising from the torsion of the $-N(CH_3)_2$ group of Prodan via a mechanism similar to that proposed for other molecules containing $-N(alkyl)_2$ groups (Grabowski et al., 1979; Braun and Rettig, 1994). Nowak et al. (1986) and Ilich and Prendergast (1989) found that the TICT electronic state lays at a sufficiently high energy level with respect to the first excited state to be considered photophysically irrelevant. This led them to conclude that a stabilization of the environment was the reason why this state was that of the lowest energies among the possible excited states (Nowak et al., 1986; Ilich and Prendergast, 1989). In all of these theoretical works, however, and depending on the authors, energetic considerations are based on different estimations of the dipole moment variation of Prodan upon excitation (Weber and Farris, 1979; Nowak et al., 1986; Balter et al., 1988).

The emitting state of Prodan has been studied by several authors who came to controversial conclusions. Rollinson and Drickamer (1980) suggested that Prodan emits from a charge transfer (CT) state in polar solvent, whereas it emits from a locally excited (LE) state in nonpolar ones. Their lifetime determinations in neat polar solvents indicated, however, the existence of a single state only. Lakowicz and Balter (1982a,b) and Lakowicz (1983) showed that the emission of Prodan in *n*-butanol at 218 K is a multistep process. Heisel et al. (1987) reported that the fluorescence of Prodan in the same solvent over the temperature range −75 to −24°C was influenced by an interaction between the solute and the solvent capable of inducing a relaxation process of the excited state. This has recently been confirmed by Sire et al. (1996), who showed an emission heterogeneity as a function of the emission wavelength. It appears that intra- and intermolecular excited-state processes may occur with this probe.

We have performed absorption, steady-state, and time-resolved fluorescence measurements of laurdan in apolar solvents and ethanol at different temperatures. The lifetime distributions were determined by maximum entropy method (MEM) analysis. The advantage of such an analysis resides in the fact that there is no a priori assumption about the number of the exponential and the sign of the preexponential amplitudes. The first set of experiments was realized in apolar white oils of different viscosities and at different temperatures in an attempt to slow down the possible intramolecular kinetic processes. The second set of experiments, realized in ethanol at different temperatures ranging from 20 to −190°C, were performed to describe the solvent relaxation effect in a more accurate manner.

This work gives experimental evidence for the existence of a reaction at the excited state for laurdan in apolar viscous oils and in frozen ethanol. The origin of this reaction is discussed in terms of intramolecular rearrangement of the probe. Moreover, the analysis of the fluorescence decays of laurdan in liquid ethanol at low temperature shows complex reactions at the excited state preceding or accompanying solvent relaxation. Time-resolved emission spectra (TRES) measurements show that the overall excited-state relaxation process is described by one major relaxation time.

MATERIALS AND METHODS

The white oils Marcol 52 and Primol 352 were obtained from ESSO (Mont Saint Aignan); laurdan was from Molecular Probes (and was used without further purification). Ethanol was purchased from Sigma, distilled the day before the experiments, and stored on molecular sieves.

Absorption spectra

The absorption spectra at temperatures ranging from 25°C to −15°C were recorded on a Lambda 2 (Perkin-Elmer) double-beam spectrophotometer. The absorption spectra at low temperatures (below −15°C) were recorded on a Cary 5 (Varian plc; Sidney) spectrophotometer, equipped for low-temperature experiments with a helium-flow cryostat (TBT, Orly, France). The bandwidth was fixed at 1 nm.

Steady-state fluorescence spectroscopy

The steady-state fluorescence spectra at room temperature were measured with a photon-counting Fluoromax fluorimeter (Spex Instruments, Jobin

Yvon, Longjumeau, France), and corrections for monochromator and source-dependent variation intensity were systematically performed.

The steady-state fluorescence emission spectra at low temperatures were recorded between 380 and 600 nm (1-nm bandwidth) for an excitation wavelength of 367 nm (2-nm bandwidth). An SLM 8000 spectrophotometer equipped with single holographic grating monochromators and Hamamatsu photon counting detectors (model H3460-53) was used. The samples were placed in a variable-temperature pourfill Janis cryostat VPF-100 (Janis Research Co., Wilmington, MA). The system consists of a cold finger, a radiation shield, an aluminum vacuum shroud, and an electrical feedthrough port. It uses liquid nitrogen in conjunction with a thermal impedance and built-in heater to operate at any desired temperature between −190°C and 50°C ± 0.5°C. Blanks were subtracted in the same experimental conditions when needed. To remove the polarization artifact, the fluorescence emission spectra were reconstructed from the four polarized spectra according to

$$I(\lambda) = I_{VV}(\lambda) + 2 \times \beta_{corr}(\lambda) \times I_{vh}(\lambda) \quad (1)$$

where $\beta_{corr}(\lambda)$ is a correction factor, defined as

$$\beta_{corr}(\lambda) = \frac{I_{hv}(\lambda)}{I_{hh}(\lambda)} \quad (2)$$

and $I_{vv}(\lambda)$, $I_{vh}(\lambda)$, $I_{hv}(\lambda)$, and $I_{hh}(\lambda)$ are the polarized fluorescence intensities (after blank subtraction) at an emission wavelength λ. The first and second subscripts refer to the orientations of the excitation and emission polarizers, respectively.

Steady-state anisotropy excitation spectra at −185°C were obtained with the same SLM-8000 spectrofluorometer operating in a T-format mode, using a Janis cryostat. The emission wavelength was selected at 430 nm (1-nm bandwidth), and the fluorescent light was selected trough interference filters (Schott; 10-nm bandwidth). The steady-state anisotropy ($A(\lambda)$) was calculated as a function of the excitation wavelength after appropriate blank subtraction:

$$A(\lambda) = \frac{I_{vv}(\lambda) - \beta_{corr}(\lambda) \times I_{vh}(\lambda)}{I_{vv}(\lambda) + 2 \times \beta_{corr}(\lambda) \times I_{vh}(\lambda)} \quad (3)$$

Fluorescence lifetime measurements

Fluorescence intensity decays were obtained by the time-correlated single photon counting technique from the polarized components $I_{vv}(t)$ and $I_{vh}(t)$ on the experimental setup installed on the SB1 beam line of the synchrotron radiation machine Super-ACO (anneau de collision d'Orsay), which has been described elsewhere (Vincent et al., 1995). The light pulse has a full-width at half-maximum of ~500 ps at a frequency of 8.33 MHz for a double-bunch mode.

Data for I_{vv} and I_{vh} were stored in separated 2K memories. The automatic sampling of the data was driven by the microcomputer. The instrumental response function was automatically recorded every 5 min by measuring the scattering of a glycogen solution for 30 s at the emission wavelength in alternation with the parallel and perpendicular components of the polarized fluorescence decay, which were cumulated for 90 s. The time resolution was in the range of 7–25 ps per channel, depending on the experiment. The shortest excited-state lifetime the instrument is able to resolve has values of 20–30 ps. For low temperature measurements, the Janis cryostat was used.

Data analysis of fluorescence lifetime distributions

Analysis of the fluorescence intensity decay data was performed by the maximum entropy method (Livesey and Brochon, 1987). The program uses MEMSYS 5 as a library of subroutines. MEMSYS 5 can also be used to handle a 150-dimension vector without any a priori assumption for each of the amplitude sign. This option was used when the classical analysis with only positive amplitudes did not provide good results in terms of χ^2 values and shape of the deviation function of the weighted residuals.

Because polarized light was used in these experiments, the total intensity decay is built by adding the parallel and twice the perpendicular components. The correction factor β_{corr} takes into account the difference of transmission of the polarized light components by the optics:

$$\begin{aligned} T(t) &= I_{vv}(t) + 2 \times \beta_{corr} \times I_{vh}(t) \\ &= E_\lambda(t) * \int_0^\infty \alpha(\tau)\exp(-t/\tau)d\tau \end{aligned} \quad (4)$$

where $E_\lambda(t)$ is the temporal shape of the excitation light pulse, * denotes a convolution product, and $\alpha(\tau)$ is the lifetime distribution, given by

$$\alpha(\tau) = \int_0^\infty \int_{-0.2}^{0.4} \gamma(\tau, \theta, A)d\theta\, dA \quad (5)$$

The recovered distribution $\alpha(\tau)$, which maximizes the entropy function S, is chosen:

$$S = \int_0^\infty \left\{ \alpha(\tau) - m(\tau) - \alpha(\tau)\log\left[\frac{\alpha(\tau)}{m(\tau)}\right] \right\} d\tau \quad (6)$$

In this expression, $m(\tau)$ is the starting model. In every analysis, a flat map over the explored (τ) domain was chosen for $m(\tau)$, because no a priori knowledge about the final distribution was available. The analysis was bound by the χ^2 constraint

$$\sum_{k=1}^{M} \frac{(I_k^{calc} - I_k^{obs})^2}{\sigma_k^2} \leq M \quad (7)$$

where I_k^{calc} and I_k^{obs} are the kth calculated and observed intensities. σ_k^2, the variance of the kth point, is equal to $\sigma_{k,vv}^2 + 4\beta^2\sigma_{k,vh}^2$ (Wahl, 1979). M is the total number of observations.

The center $\langle\tau\rangle$ of a single class j of lifetimes over the $\alpha(\tau_i)$ distribution was defined as

$$\langle\tau\rangle = \frac{\sum_i \alpha_i(\tau_i)\tau_i}{\sum_i \alpha_i(\tau_i)} \quad (8)$$

where the summation is performed on the significant values of the $\alpha(\tau_i)$ for the j class. C_j is the normalized contribution of the lifetime class j. The broadness w_j of the distribution was calculated according to

$$W_j = \left[\frac{\sum_i \alpha_i(\tau_i - \langle\tau_j\rangle)^2}{\sum_i \alpha_i} \right]^{1/2} \quad (9)$$

Time-resolved fluorescence emission spectra: collection and analysis

TRES were reconstructed in each experimental condition from 17 individual decays as a function of the emission wavelength from 390 up to 550 nm (bandwidth between 2 and 10, depending on the experiment), with a 10-nm step. Each decay was fit with the MEM program, using the classical or the negative amplitude option, to gain the best fit in terms of χ^2. The integral of each decay curve was normalized to the corresponding steady-state fluorescence emission wavelength recorded on the same instrument with identical experimental conditions. By collecting the vertical (I_{vv}) and the horizontal (I_{vh}) fluorescence intensity components and by taking into account the β correction factor, the calculated impulse fluores-

cence intensity (Eq. 4) as well as the steady-state intensity ($I_{vv} + 2\beta I_{vh}$) are de facto corrected for the difference in transmission of the polarized light components by the optics. For the quantitative description of the spectral shift, the barycenters in frequency were computed and the full widths at half-peak were calculated from the raw spectra. The shift function $C(t)$ was defined classically as (Bagchi, 1989)

$$C(t) = \frac{\bar{\upsilon}_t - \bar{\upsilon}_\infty}{\bar{\upsilon}_0 - \bar{\upsilon}_\infty} \quad (10)$$

where $\bar{\upsilon}_t$, $\bar{\upsilon}_0$, and $\bar{\upsilon}_\infty$ are the barycenter values in frequency at times t, 0, and ∞, respectively. Reaction kinetics were determined from a MEM analysis of $C(t)$ as a sum of exponentials (Chapman et al., 1990):

$$C(t) = \sum_j a_j e^{-t/\tau_{Rj}} \quad (11)$$

Viscosity measurements

The temperature dependence of the oil viscosities between 5°C and 40°C was determined on a controlled stress Rheometer (RS100; Haake) with cylindrical geometry (Z41).

RESULTS

To obtain information on the photochemistry and photophysics of laurdan (Fig. 1 *B*), this fluorescent probe has been studied by steady-state and time-resolved fluorescence measurements in two types of neat solvents, i.e., apolar white and viscous oils (Marcol and Primol), on one hand and in polar solvent (ethanol) as a function of temperature on the other.

Apolar white and viscous oils: Marcol and Primol

The white apolar oils Marcol and Primol have different viscosities at room temperature (13 mPas and 210 mPas, respectively) (Table 1). Absorption and fluorescence spectra on one hand and fluorescence decays on the other have been analyzed for laurdan in these viscous oils.

Absorption, excitation, and emission spectra of laurdan in apolar solvents (Marcol and Primol)

The absorption spectra of laurdan (8 μM) in Primol (Fig. 2 *A*) and in Marcol (data not shown) at 20°C are broad and similar, indicating that the ground states of laurdan in the two oils are identical. These spectra were best fitted by three symmetrical Gaussian bands centered at ~325 nm, 348 nm, and 374 nm (Fig. 2 *A*).

The excitation spectra are similar to the absorption spectra (data not shown) and exhibit a maximum at 343 nm, whatever the oil used. The emission spectra of laurdan (8 μM) in Marcol and Primol at 20°C and −5°C are presented in Fig. 2 *B*. They are broad and asymmetrical, and the maximum of the spectrum (389 nm) is followed in the red part by a shoulder at ~400 nm. The relative intensity I_{max}/I_{400} increases slightly with the viscosity and the temperature (Fig. 2 *B*, *inset*).

Fig. 3 represents the emission spectra of laurdan in Primol recorded at different excitation wavelengths, i.e., from the wavelength at the maximum of the excitation spectrum (343 nm) to its very red edge (395 nm) (Fig. 3, *inset*). As the

TABLE 1 Results of the MEM decay analysis performed on laurdan (8 μM) in Primol, Marcol, and cyclohexane as a function of the temperature and emission wavelength (Fig. 4)

	λ_{em}	t		τ_1		τ_2		τ_{mean}	Viscosity
	(nm)	(ps)	Surface	(ps)	Surface	(ps)	Surface	(ps)	(mPa s)
Primol	375	—	—	84	25.74	189	72.65	162	
40°C	390	15	22.83*	119	39.35	223	34.79	168	67
(Fig. 4A)	450	16	49.05*	115	34.36	236	16.01	153	
Primol	375	—	—	143	49.49	254	50.51	199	
20°C	390	23	9.41*	140	35.08	257	54.84	211	210
(Fig. 4B)	450	23	37.47*	132	30.61	269	29.57	199	
Primol	375	15	35.75	190	30.52	339	33.59	268	
−05°C	390	16	16.84*	130	27.50	329	54.68	262	ND
(Fig. 4C)	450	17	37.95*	117	24.38	339	36.66	250	
Marcol	375	—	—	113	28.86	197	70.86	173	
20°C	390	23	12.84*	—	—	—	—	175	13
(Fig. 4D)	450	19	45.07*	123	37.63	239	17.29	160	
Marcol	375	—	—	—	—	—	—	220	
−05°C	390	15	05.41*	120	23.94	263	67.07	225	ND
(Fig. 4E)	450	18	48.04*	88	24.37	269	24.96	180	
Cyclohexane	388	15	33.07*	—	—	—	—	93	1

* Negative amplitudes.

τ_{mean} is the average between τ_1 and τ_2 weighted by the surfaces.

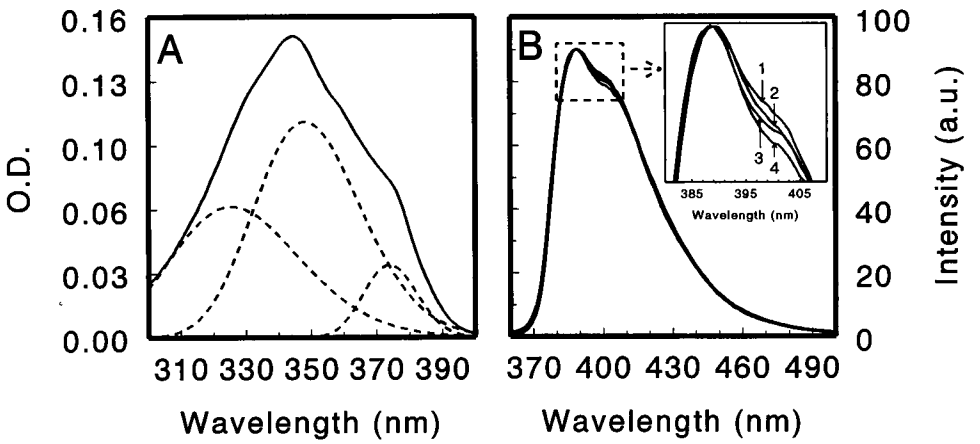

FIGURE 2 (*A*) Absorption spectrum of laurdan (8 μM) in Primol (20°C). The fit has been realized with three symmetrical Gaussian bands (λ_{max1} = 325 nm, halfwidth1 = 1857 cm^{-1}, I_{max1} = 0.066; λ_{max2} = 348 nm, halfwidth2 = 1336 cm^{-1}, I_{max2} = 0.108; λ_{max3} = 374 nm, halfwidth3 = 579 cm^{-1}, I_{max3} = 0.036). (*B*) Emission spectra of laurdan (8 μM) in Marcol at 20°C (*1*) and −05°C (*3*) and in Primol at 20°C (*2*) and −05°C (*4*).

excitation is moved toward the red, the emission spectra first change in shape and then are red shifted. The relative intensity of the red shoulder of the emission spectra increases compared to that of the maximum, indicating a photoselection of the low-energy-emitting component. This evolution of the emission spectra with the excitation wavelength was also observed for laurdan in Marcol (data not shown).

Fluorescence decays of laurdan in the nonpolar oils Marcol and Primol at different temperatures: characterization of the kinetic parameters

Fluorescence decays of laurdan in Primol and Marcol (8 μM) have been recorded at different temperatures. The decay analyses are shown in Fig. 4: for laurdan in Primol (40°C, 20°C, and −5°C: Fig. 4, *A*, *B*, and *C*, respectively) and laurdan in Marcol (20 and −5°C: Fig. 4, *D* and *E*, respectively). The decays were recorded using λ_{exc} = 344 nm (wavelength at the maximum of the excitation spectrum) and three different emission wavelengths situated in the blue edge (λ_{em} = 375 nm), at the maximum (λ_{em} = 390 nm), and in the red edge (λ_{em} = 475 nm) of the spectrum.

The analyses were systematically performed with the classical program (only positive amplitudes). The optional program without any a priori assumption on the amplitude sign was only used when the previous analysis was not good in terms of χ^2 values and the shape of the deviation function of weighted residuals.

In all of these different decays, the analysis by the classical program was only possible when the emission wavelength was situated in the blue edge of the spectrum and in some cases at the maximum, whereas for an emission wavelength situated in the red edge of the emission spectrum, the analysis provides the correct fit only with the negative-amplitude option. A negative amplitude indicates that before the radiative deexcitation, a fast reaction compared to the emission lifetime exists, leading to an increase in the emitting population observed by fluorescence.

As a general rule, whatever the temperature and the emission wavelength, the lifetime distribution exhibits two

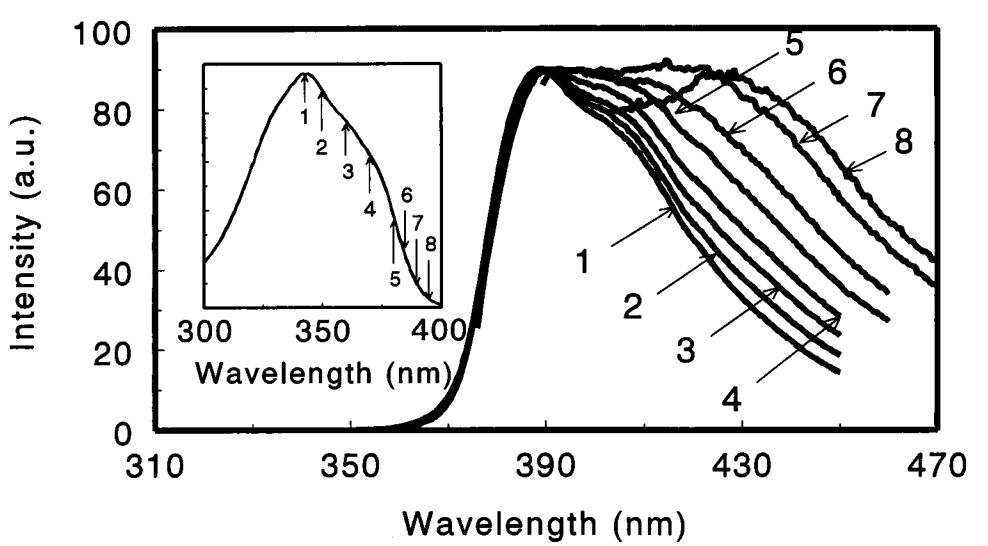

FIGURE 3 Emission spectra of laurdan (8 μM) in Primol obtained with an excitation wavelength of 343 nm (*1*), 350 nm (*2*), 360 nm (*3*), 370 nm (*4*), 380 nm (*5*), 385 nm (*6*), 390 nm (*7*), and 395 nm (*8*) (T = 20°C). The inset represents the excitation spectrum of laurdan (8 μM) in Primol (T = 20°C), and the arrows indicate the wavelength at which the excitations were performed.

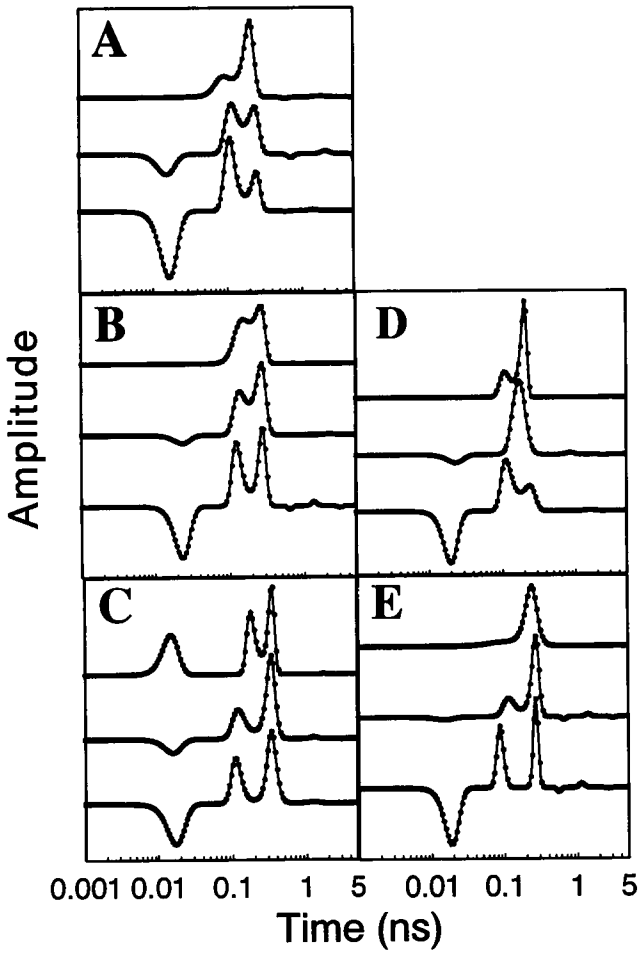

FIGURE 4 MEM recovered lifetime distributions of laurdan (8 μM) in Marcol and Primol as a function of temperature and emission wavelength. In every chart the three distributions were obtained with an excitation performed at 344 nm and an emission wavelength of 375 nm for the upper curve, 390 nm for the middle curve, and 450 nm for the lower curve. The experiments were carried out in Primol at 40°C (*A*), 20°C (*B*), and −5°C (*C*) and in Marcol at 20°C (*D*) and −5°C (*E*). See Table 1 for details.

"slow" components (in the subnanosecond time range), most often preceded by a very short one (~20 ps) (Table 1). The sign and the amplitude of this last depend on the emission wavelength. In the blue edge, this component is only visible for laurdan in Primol at −5°C (the most viscous medium) (Fig. 4 *C*), whereas the lifetime distribution obtained under the other conditions (temperatures and oils) did not exhibit any short component. When the emission wavelength is shifted toward the red, a short component of 20 ps with a negative amplitude appears. Its amplitude increases with the emission wavelength.

The two slow time components depend on viscosity, i.e., they tend to increase with the viscosity (Table 1). Their relative proportions depend on the emission wavelength: in almost all cases, the redder the emission wavelength, the higher the proportion of the faster component. This tends to indicate that the lifetime of the lowest energy excited state is shorter than that of the highest energy excited state. In Table 1 is also reported the result of the MEM analysis, which was made for the fluorescence decay of laurdan dissolved in cyclohexane. It shows, as in the oils, a very fast component of ~15 ps with a negative amplitude. However, only one lifetime distribution of 93 ps is detectable, in contrast to the oils, for which two components are resolved. This may be due to the fact that in cyclohexane (viscosity 1 mPas), the lifetimes are too fast and similar to be distinguished.

Polar media as a function of temperature

Effect of temperature on the absorption and emission spectra of laurdan in ethanol

In Figs. 5 and 6, respectively, are reported the absorption (recorded between 20°C and −110°C) and the emission spectra (recorded between 20 and −190°C) of laurdan.

The absorption spectra are asymmetrical; their intensities, widths, and maximum wavelengths depend on temperature (Fig. 5 *A*). Changes in intensity and maximum wavelength are likely connected to the changes in dielectric constant and refractive index experienced by ethanol upon cooling. Indeed, as documented in many theoretical works, these properties of the solvent strongly influence the absorption transition of the solute molecule (Buckingham, 1958). The width decrease in the spectra may be explained by the decrease in vibrational motion as a function of the temperature decrease.

As the temperature is decreased, a red shift of the absorption maximum (365.5 nm at 25°C and 375.5 nm at −110°C) is detected. To get an insight into the broad shape of the absorption spectra that is visible whatever the temperature, deconvolution of these spectra with Gaussian curves has been performed. As for the absorption spectra of laurdan in oils (see previous section), three symmetrical Gaussian curves were necessary to deconvolute the spectra (Fig. 5, *B* and *C*, for laurdan at 20°C and −110°C, respectively). This again underlines the heterogeneity of the ground state, which is visible for all temperatures. For the two reddest Gaussian curves, their maxima (365 nm and 387 nm) and width (1795 cm^{-1} and 820 cm^{-1}) remain constant, whereas their intensity increases when the temperature is decreased. For the third Gaussian curve, the intensity, the width, and the maximum (341 nm at 25°C and 331 at −110°C) change.

The excitation polarization spectrum of laurdan in ethanol at −185°C has been recorded (data not shown). From the blue to the red edge of spectrum, the anisotropy changes from 0.3 to 0.4, indicating that at this temperature at least two transitions are involved in the fluorescence excitation spectrum.

In Fig. 6 are reported the emission spectra of laurdan at different temperatures. The areas of the emission spectra of laurdan between 20°C and −190°C have been normalized. From 20°C to −50°C the emission spectra remain symmetrical and are red shifted without important changes in their

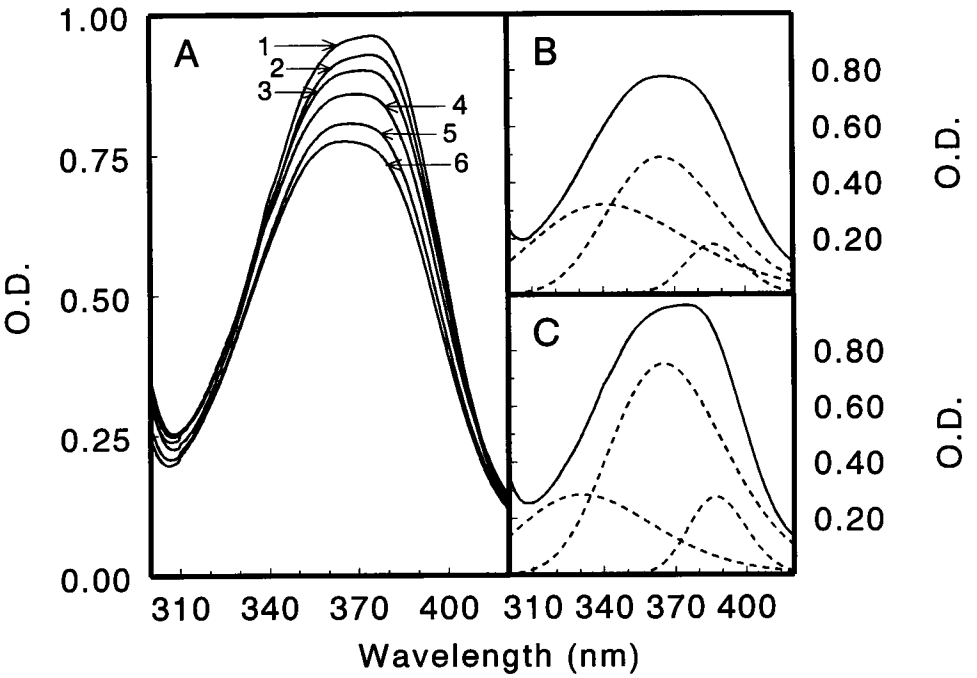

FIGURE 5 (*A*) Absorption spectra of laurdan in ethanol at −108°C (*1*), −77°C (*2*), −48°C (*3*), −20°C (*4*), 0°C (*5*), and 25°C (*6*). (*B* and *C*) Absorption spectra of laurdan in ethanol at −108°C (*B*) and 25°C (*C*). Each of these spectra has been fitted with three Gaussian bands (see the text for more details).

width (Fig. 6 *B*). Below −50°C the spectra are not only blue shifted but become asymmetrical: two fluorescence bands appear, separated by an isoemissive point at λ_{em} = 473 nm (Fig. 6 *A*). The wavelengths at the maxima of the two spectra are centered at ~450 nm and 490 nm. Finally, at −190°C, the emission spectrum is further blue shifted compared to the spectrum at −110°C, i.e., centered at 418 nm (Fig. 6 *A*). The maximum of the emission spectrum at −190°C depends on the excitation wavelength (Fig. 6 *A*, *inset*), i.e., this maximum is slightly blue shifted for an excitation at 330 nm and red shifted for an excitation at 405 nm. For the red excitation wavelength, the emission spectrum is centered at 435 nm (red shift of ~20 nm).

Effect of temperature on the time-resolved fluorescence of laurdan in ethanol

Fluorescence decays were recorded by using a fixed excitation wavelength (λ_{exc} = 367 nm) and different emission wavelengths corresponding to the blue edge (Fig. 7 *A*) and to the red edge (Fig. 7 *B*) of the corresponding emission spectrum for temperatures ranging from 20°C to −190°C.

For the fluorescence decays recorded in the blue edge of the emission spectra (Fig. 7 *A*), MEM recovered lifetime distributions showed complex kinetics associated to the fluorescence decays. From 20°C to −50°C, only one short component is observed, followed by the lifetime of the

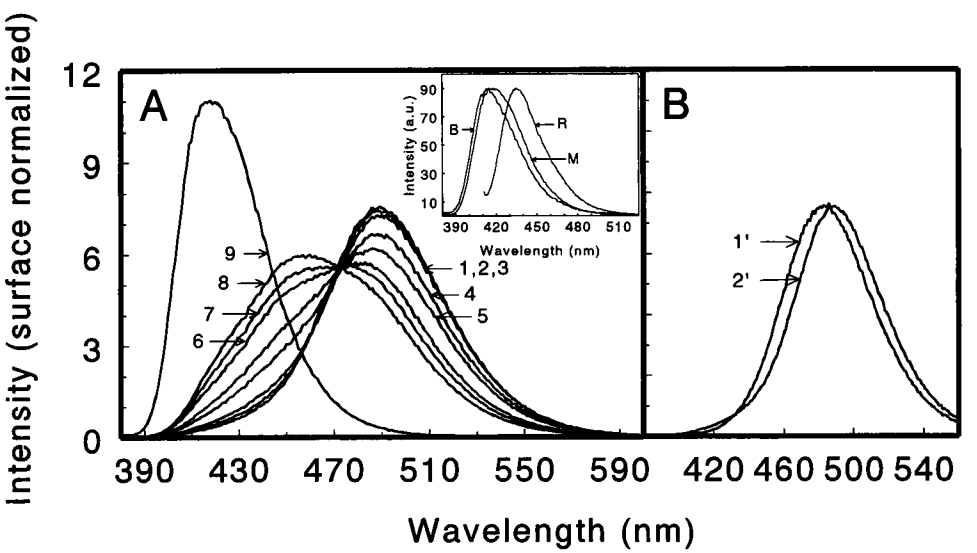

FIGURE 6 (*A*) Emission spectra of laurdan (6 μM) in ethanol at −50°C (*1*), −60°C (*2*), −70°C (*3*), −80°C (*4*), −85°C (*5*), −90°C (*6*), −100°C (*7*), −110°C (*8*), and −190°C (*9*). All of the excitations were performed at 367 nm. The inset represents the emission spectra of laurdan at −190°C obtained with an excitation performed at 330 nm (B), 367 nm (M), and 405 nm (R). (*B*) Emission spectra of laurdan (6 μM) in ethanol at 20°C (1′) and −40°C (2′) obtained with an excitation performed at 367 nm.

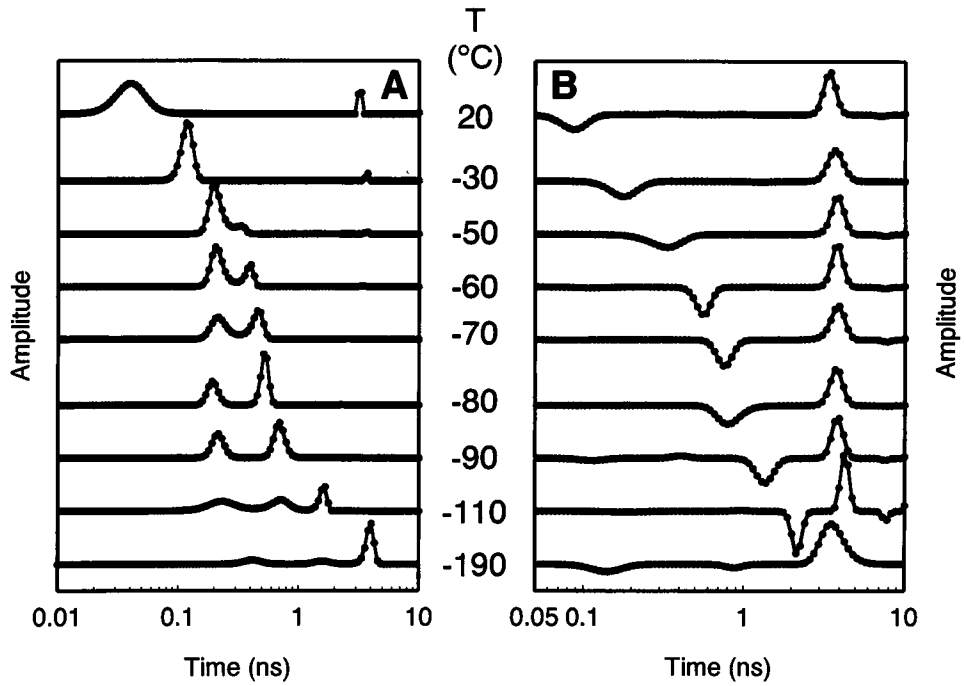

FIGURE 7 MEM recovered lifetime distributions of laurdan in ethanol (6 μM) as a function of temperature. (*A*) The decays were obtained with an excitation performed at 367 nm and, from the top to the bottom, at 20°C (λ_{em} = 440 nm, t_1 = 56 ps, t_2 = 3.2 ns), −30°C (λ_{em} = 440 nm, t_1 = 117 ps, t_2 = 3.66 ns), −50°C (λ_{em} = 430 nm, t_1 = 207 ps, t_2 = 331 ps, t_3 = 3.65 ns), −60°C (λ_{em} = 430 nm, t_1 = 213 ps, t_2 = 380 ps), −70°C (λ_{em} = 430 nm, t_1 = 222 ps, t_2 = 446 ps), −80°C (λ_{em} = 420 nm, t_1 = 195 ps, t_2 = 523 ps), −90°C (λ_{em} = 430 nm, t_1 = 216 ps, t_2 = 702 ps), −110°C (λ_{em} = 405 nm, t_1 = 240 ps, t_2 = 704 ps, t_3 = 1.68 ns) and −190°C (λ_{em} = 380 nm, t_1 = 422 ps, t_2 = 1.59 ns, t_3 = 3.89 ns). (*B*) The decays were obtained for the same temperatures and the same excitation wavelength, but with an emission wavelength of 550 nm in all cases, except for ethanol at −190°C (λ_{em} = 530 nm) (see Table 2 for the MEM recovered lifetime distribution parameters).

fluorophore. Whereas this last component is independent on temperature, its proportion drastically decreases with temperature and cancels out below −50°C. Meanwhile, the short component becomes longer as the temperature is decreased. A further decrease in temperature induces the appearance of a second component. From −50°C to −90°C, the distributions consist of a nearly unchanged component situated around 210 ps, along with a second component that increases from 330 ps (at −50°C) to 700 ps (at −90°C). In nearly frozen ethanol (−110°C), a third component is obtained. Finally, in frozen ethanol (−190°C), for which the solvent relaxation process is forbidden, three different temporal components with positive amplitudes are evidenced by the MEM analysis of the decay.

In the red edge of the fluorescence emission spectra (Fig. 7 *B*), and for temperatures ranging from 20°C to −110°C, the MEM recovered lifetime distributions are composed of only two components, whatever the temperature considered. The long time constant is only slightly thermal sensitive and is affected by a positive amplitude, whereas the short time constant is strongly thermal sensitive and is affected by a negative amplitude (Table 2). This suggests that this short time constant is "relaxational." From its thermal evolution, an Arrhenius plot was constructed (Table 2). It allows the determination of the activation energy of ethanol dipolar relaxation, which was found to be 3 kcal/mol. This value is on the same order of magnitude as that obtained with other probes, but smaller than the values provided by dielectric measurements. The absolute value of the "relaxational" component is not in agreement with the longitudinal relaxation time value (Fröhlich, 1958) or with that of the microscopic relaxation time (Madden and Kivelson, 1984).

TABLE 2 MEM recovered lifetime distributions of fluorescence decays obtained for laurdan (6 μM) in ethanol (λ_{exc} = 367 nm and λ_{em} = 550 nm) at different temperatures (Fig. 7 *B*)

Temperature (°C)	Relaxational time (τ_{rel}, ps)	Corrected time (τ_{cor}, ps)	Lifetime (τ_f, ns)
20	85	87	3.46
−30	180	189	3.76
−50	327	357	3.86
−60	560	656	3.84
−70	765	956	3.83
−80	834	1069	3.79
−90	1365	2109	3.87
−110	2142	4300	4.27

The relaxational time constant has been corrected according to the following equation (cf. Vincent et al., 1995): $1/\tau_{rel} = 1/\tau_{cor} + 1/\tau_f$. From these corrected values (τ_{cor}), an Arrhenius plot was carried out, giving an activation energy of the relaxation process of 3 kcal/mol. The correlation factor of the linear regression was 0.992.

Concerning the analysis of the fluorescence decay of laurdan in ethanol at −190°C and recorded in the red edge of the emission spectrum, three temporal components are determined (as in the blue edge). Two of these components have negative amplitudes and are followed by a third and longer one (3.7 ns) with a positive amplitude.

TRES measurements performed in ethanol in the liquid phase (at −80°C) evidence a large red shift of the fluorescence emission spectrum as a function of time (Fig. 8). The variation of the barycenter of the fluorescence emission spectra shows a large decrease as a function of time from 22,500 cm^{-1} to 20,000 cm^{-1}. A maximum shift of 2500 cm^{-1} is was therefore observed, which corresponds to a stabilization energy of the excited state of ~7.1 $kcal \cdot M^{-1}$. The logarithmic representation of the $C(t)$ function shows a major straight line, indicating that its variation can be described by a major exponential decay (Fig. 9, *inset*). A small contribution of a shorter time can also be seen. MEM analysis of the $C(t)$ function as a sum of 100 exponentials confirms this observation (Fig. 9). The TDFS is described mainly by a major nanosecond time constant that accounts for 90% of the excited-state energy loss (Fig. 9). The initial picosecond decay accounts for 10% of the energy variation. Such a multiexponential behavior of $C(t)$ has often been observed with other dyes that do not exhibit intramolecular excited-state reactions, like coumarin 153 (Horng et al., 1995). During the course of the spectral shift, a transient change in the spectral shape is also observed, which is manifested by a transient increase in the spectral half-width at intermediate times (Fig. 9, *inset*). This observation is compatible with the existence of a continuous shift from a homogeneous emission spectrum at short times and heterogeneous ones at intermediate times, where incomplete relaxation shells of different types are likely occurring. This transient broadening reflects the heterogeneity of both excited states and of solute-solvent interactions when the solvent relaxation is not fully completed.

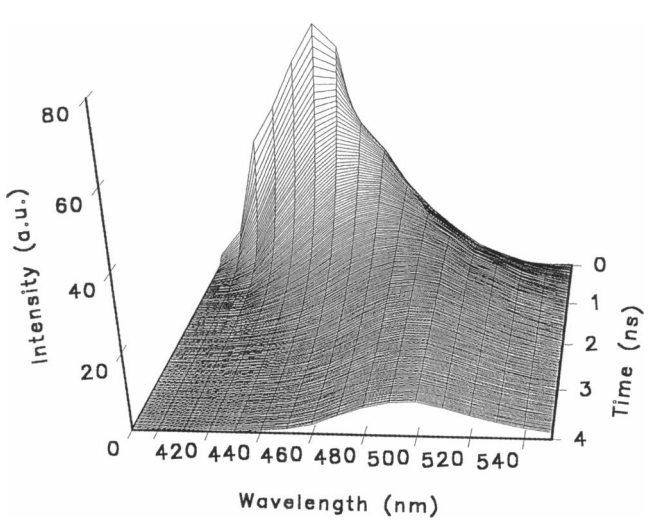

FIGURE 8 Three-dimensional representation of a TRES experiment corresponding to laurdan (6 μM) in ethanol at −80°C. Each emission spectrum is reconstructed by steps of 20 ps.

Whereas analysis of the TDFS provides information about the major relaxation processes that contribute to the excited-state energy loss, examination of the time constant distribution describing the fluorescence decay curves at different emission wavelengths allows us to detect the different excited-state emission kinetics that are in competition with the relaxation kinetics. Both sets of information are contained in the individual decays. They can therefore contribute additional information on the excited state behaviors of the probe. In fact, it should be emphasized that observation of a TRES is not always sufficient to draw definite conclusions about the existence of a solvent-induced spectral relaxation. An excited-state lifetime heterogeneity can result in such an apparent spectral shift with time if, for instance, short-lived excited states emit preferentially in the blue spectral region and long-lived ones dominate in the red region of the emission spectrum.

The examination of the evolution of the time constant distributions recovered by MEM as a function of the emission wavelength shows great complexity (Fig. 10). It is possible to distinguish, however, two spectral regions where this evolution exhibits characteristic features: the blue edge of the emission spectrum and the red edge. In the blue edge, only two time constants are separated. They do not correspond to any time constants detected in the red edge. Even the longest emitting lifetime in the red edge is not visible at all in the extreme blue edge. With increasing emission wavelength, the value of the long time constant in the blue edge region of emission increases. Its relative contribution increases too, then decreases, and finally disappears in the middle range of emission energies. The evolution of the value of this time constant suggests a heterogeneity of fluorescence excited states when going from the first unrelaxed state to more stable solvent-relaxed ones, via the establishment of the CT. Its disappearance may indicate the existence of different mechanisms of relaxation occurring at different times and corresponding to different stabilization energies of the excited states. The shorter time constant observed in the blue edge of the fluorescence spectrum progressively disappears in the middle range of the spectrum. It may be a combination of spectral shifts and spectral deformation, inasmuch as the TRES shows a large, fast broadening of the fluorescence emission spectrum as a function of time.

In the red edge, the situation appears simpler. Two time constants affected with negative amplitudes are observable with the long-lived emission. The shortest time constant contributes more in the middle region of the emission spectrum, whereas the longest one is only visible at the far red edge. Both display respective values very close to those calculated from the TRES analysis, and they should therefore represent the same relaxation processes that appear to dominate the spectral shift and thus are responsible for all of the measurable stabilization energy of the excited state.

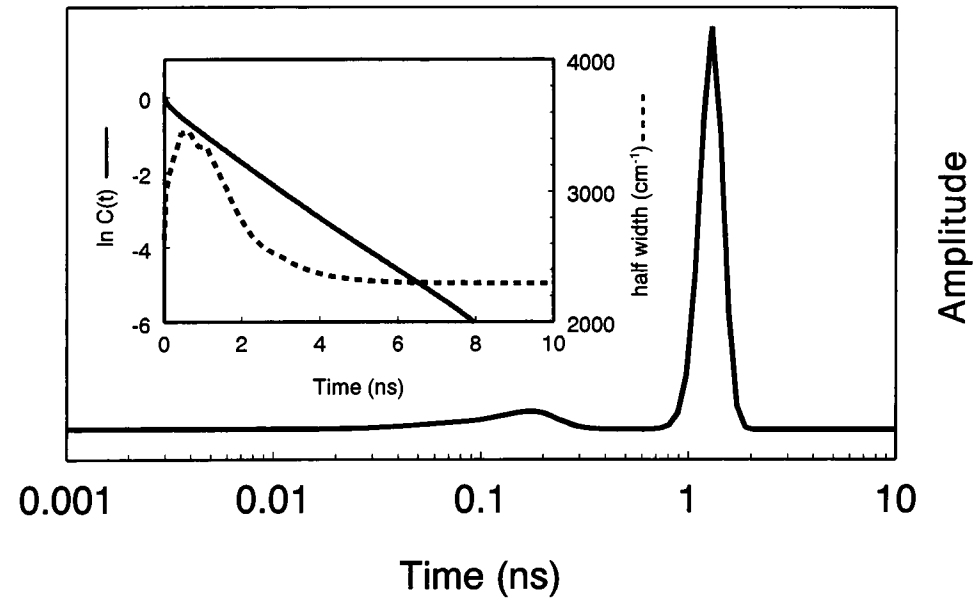

FIGURE 9 MEM analysis of $C(t)$ obtained from the TRES experiment (see Materials and Methods for more details). The inset represents the evolution of the half-width and of $\ln(C(t))$ obtained from the reconstructed spectra from t = 0–10 ns.

DISCUSSION

Despite the large number of reported experimental data, the origin of the high sensitivity of laurdan to environmental changes during lipidic phase transition still remains unclear. Static and time-resolved fluorescence and absorption experiments in apolar and polar media have been realized to gain insight into the photochemistry and photophysics of laurdan.

The absorption spectra of laurdan are generally broad and asymmetrical. Ilich and Prendergast (1989), by semiempirical calculation, proposed that the absorption spectrum of Prodan, which is the prolyl derivative of laurdan (Fig. 1 *A*), could be characterized by three different electronic transitions. The first two electronic transitions (centered at 355 and 365 nm) would correspond to the $\pi^*\leftarrow\pi$ absorption band of the naphthalene ring, the twinning being induced by the fact that the two highest occupied molecular orbitals in Prodan are of the same naphthalene HOMO parentage. The third one (centered at 388 nm) would correspond to a $\pi^*\leftarrow n$ absorption band. Consistent with this hypothesis, three Gaussian curves were necessary to decompose the absorption spectra of laurdan whatever the solvent used, i.e., polar or apolar. The different maxima of the three Gaussian curves depend, however, on the solvent used, indicating an influence of the solvent on the absorption transitions. Recently Sire et al. (1996) have interpreted the absorption spectra of 4-2′-(dimethylamino)-6′-naphtoylcyclo-hexanecarboxylic acid (DANCA), which is also a naphthalene derivative (Fig. 1 *C*), according to Ilich and Prendergast (1989). They used two Gaussian curves to decompose the spectra recorded in different neat solvents and attributed these two absorption bands to $\pi^*\leftarrow\pi$ and $\pi^*\leftarrow$n transitions. The maxima of the Gaussian curves, centered at ~350 nm and 380 nm, were also shifted, depending on the solvent.

The absorption spectra of laurdan in ethanol are slightly red shifted with decreasing temperature down to −110°C. As for apolar solvents, three Gaussian curves were necessary to fit all of these different spectra. Moreover, the evolution of the anisotropy from 0.3 to 0.4 for laurdan in frozen ethanol supports the idea that at least two transitions are involved in the excitation spectrum.

No clear correlation between the red shift of the absorption spectra with the decrease in temperature and the change in proportions of the Gaussian components can be established, however. Therefore, from these deconvolutions, it was not possible to attribute the modification of the spectrum with temperature to a stabilization of one of the transitions.

However, in an attempt to determine whether this absorption heterogeneity may arise from heterogeneity of the fundamental state, Raman spectroscopy has been performed on crystallized laurdan and dissolved either in aprotic (tetrahydrofuranne) or in protic (ethanol) solvents. The preliminary results (data not shown) indicate that the molecule, crystallized or dissolved in these two types of solvent, is plane, the C═O being always strongly conjugated to the naphthalene rings. This result is in agreement with the calculations of Ilich and Prendergast (1989). In ethanol the C═O does not appear to be protonated, but a dynamic distribution of hydrogen bonding is observed. Further spectral differences are observed, but cannot be straightforwardly attributed to conformational changes, as the hydrogen bond pattern observed may influence the vibrational mode inducing the nuclear coordinate of the C═O groups. More experiments are already being undertaken to determine the precise conformation of laurdan in ethanol. In a first interpretation, however, we cannot say that the absorption heterogeneity originates from a heterogeneity of the fundamental state.

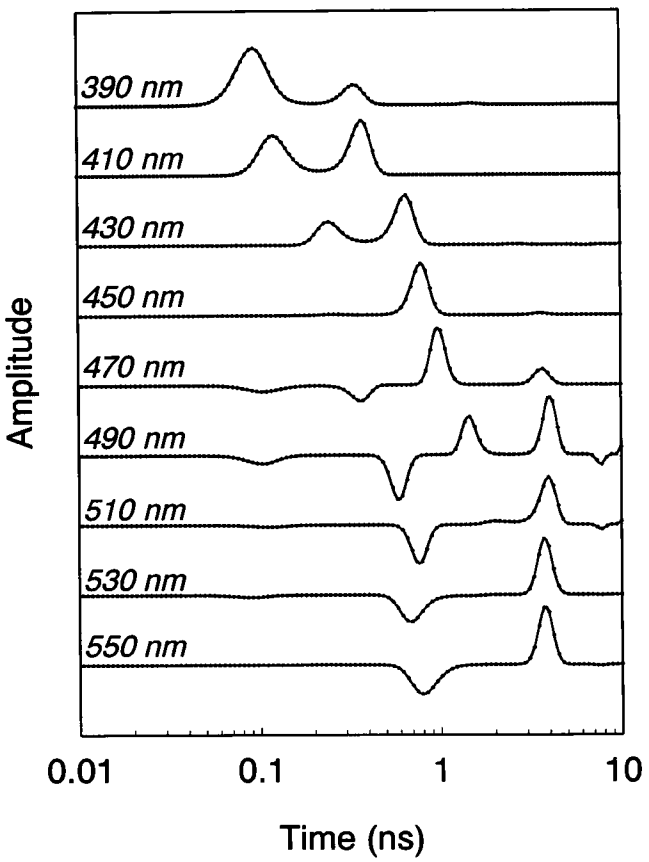

FIGURE 10 MEM recovered lifetime distributions of laurdan in ethanol (6 μM) at −80°C as a function of the emission wavelength. The decays were obtained with an excitation performed at 367 nm and, from the top to the bottom, at λ_{em} = 390 nm (t_1 = 101 ps, t_2 = 346 ps), λ_{em} = 410 nm (t_1 = 128 ps, t_2 = 363 ps), λ_{em} = 430 nm (t_1 = 258 ps, t_2 = 636 ps), λ_{em} = 450 nm (t_1 = 270 ps, t_2 = 784 ps, t_3 = 3.64 ns), λ_{em} = 470 nm (t_1 = 109 ps, t_2 = 357 ps, t_3 = 995 ps, t_4 = 3.67 ns), λ_{em} = 490 nm (t_1 = 103 ps, t_2 = 591 ps, t_3 = 1.48 ns, t_4 = 4.02 ns), λ_{em} = 510 nm (t_1 = 111 ps, t_2 = 767 ps, t_3 = 2.09 ns, t_4 = 3.86 ns), λ_{em} = 530 nm (t_1 = 88 ps, t_2 = 749 ps, t_3 = 3.78 ns), and λ_{em} = 550 nm (t_1 = 834 ps, t_2 = 3.79 ns).

Fluorescence of laurdan in apolar media

The steady-state fluorescence measurements show that the half-width and the wavelength at the maximum of the emission spectra of laurdan in apolar media drastically depend on the excitation wavelength. The observed red edge effect is the signature of a spectral heterogeneity, which can be of static or dynamic origin. The fluorescence decays analyzed by MEM (Table 1) show a very short component (~20 ps) followed by two longer components. The sign and the amplitude of the very short component depend on the emission wavelength and would correspond to the kinetic constant of the reaction at the excited state. This kinetics is very fast and is at the limit of the instrumentation (Vincent et al., 1995), but seems to be significant. The double exponential describing the fluorescence decays is likely due to the respective emissions of the interconverting excited states.

The origin of the excited-state reaction in apolar solvents has been examined in the literature (Ilich and Prendergast, 1989; Bunker et al., 1993; Nowak et al., 1986), and the possibility of fluorescence from twisted intramolecular charge transfer states (TICT) was considered. Experimentally, the existence of a classical TICT fluorescent state is still debated and has not been definitively proved (Bunker et al., 1993). But in light of semiempirical calculations for Prodan, Ilich and Prendergast (1989) come to the conclusion that the TICT states are energetically unfavorable in an apolar environment. However, the same authors established a sequence of plausible structural, conformational, and electronic density distribution changes in the lowest singlet excited state. This scheme postulates that the electronically excited chromophore first undergoes a structural change, leading to a quasiseparation of the N-$(CH_3)_2$ fragment. Twisting of the amino group, the conformational requirement identified by solvatochromic measurements, occurs in a second step. This step is a prerequisite for the completeness of the CT state. Whereas this second step is considerably stabilized by polar solvents, the first step, involving ring distortion, may take place, even in apolar solvents. We should also remark that conjugation of the carbonyl group with the naphthalene ring and the nitrogen atom is also important for the full charge separation in the final CT state. This suggests that CT states with different dipole moments can be formed as a function of time. A time-dependent dipole moment can therefore be seen by the solvent cage (Declémy and Rullière, 1994).

Whatever the mechanisms of the reactions at the excited state are, we can suggest that the very fast kinetics (k_i), determined by MEM analysis of the decays, likely describes an interconversion reaction between the two excited states that have been previously called by Rollinson and Drickamer (1980) "locally excited" (LE) and "charge transfer" (CT) states: these two states originate in the heterogeneity of the absorption transitions, i.e., $\pi^* \leftarrow \pi$ and $\pi^* \leftarrow$n transitions, respectively (Fig. 11 *A*). The two longer lifetime distributions determined by MEM analysis could then correspond to the radiative deexcitation of the LE and CT excited states, k_{LE} and k_{CT}, respectively, in Fig. 11 *A*. Moreover, the evolution of the proportion of these two long components with emission wavelength and temperature tends to indicate that the shorter lifetime can be assigned to the radiative deexcitation of the CT state (k_{CT}) and the longer one to the deexcitation of the LE state (k_{LE}).

Fluorescence of laurdan in polar media

In addition to intramolecular excited-state reactions, the fluorescence of laurdan in ethanol shows evidence of a predominant solvent relaxation process. Steady-state emission spectra have been recorded for temperatures ranging from 20°C to −190°C to observe the consequence of the slowing down of the solvent relaxation kinetics for the inter- and intramolecular relaxation processes.

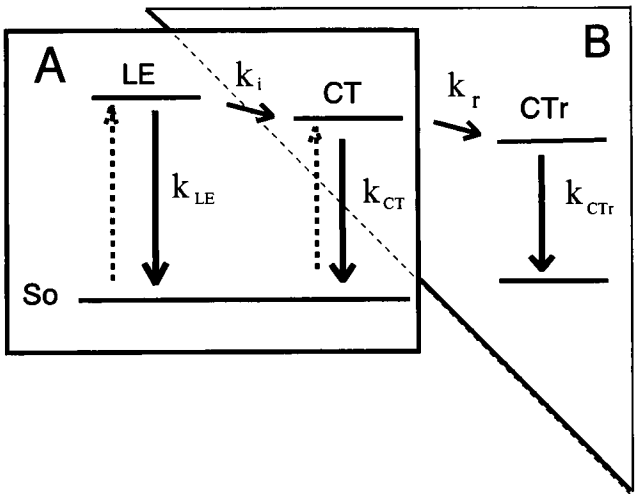

FIGURE 11 Schematic representation of the possible deexcitation pathway of Laurdan. (*A*) → kinetics evidenced for laurdan in the apolar oils and supposed in frozen ethanol. (*B*) → kinetics evidenced for laurdan in ethanol for red emission wavelength.

The red shift of the emission spectrum from 20°C to −50°C can be accounted for by the fact that thermal energy can prevent complete alignment of the solvent dipoles around the excited state (Macgregor and Weber, 1981). At −50°C, the stabilization of the excited state by the solvent relaxation is at maximum, and the emission spectra are then red shifted down to this temperature. The half-width is only slightly decreased, which is in agreement with more homogeneous solvent shells at lower temperatures, due to the ordering effect of the dipolar interactions that become stronger than the thermal motion.

Between −50°C to −110°C, two emission bands separated by an isoemissive point appear. This behavior has already been observed by Merlo and Yager (1990) for laurdan incorporated into DPPC membranes during the temperature-dependent gel-to-fluid liquid phase transition. To our knowledge, however, it has never been observed in neat solvents. This phenomenon indicates that on the average, two major excited states are interconverting in this temperature range. As the temperature is decreased, the relaxation kinetics is slowed down. The two emission spectra would then correspond to the fluorescence of the relaxed and unrelaxed charge transfer states (CTr and CT, respectively) (Fig. 11 *B*).

In frozen ethanol (−190°C), the emission spectrum is further blue shifted compared to the one at −110°C, but remains at longer wavelengths than in apolar solvents. Moreover, the fact that the maximum of the emission spectra in frozen ethanol depends on the excitation wavelength indicates the existence of an emission heterogeneity. This heterogeneity could then partly arise from the radiative deexcitation of the LE and CT states (Fig. 11 *A*). Our conclusion from these static fluorescence measurements is that there are three different emitting populations, corresponding to CT, CTr, and LE states (Fig. 11).

Time-resolved fluorescence decays and TRES measurements provide more information about the excited-state heterogeneity and the different excited-state reactions. For emission wavelengths situated at the extreme red edge of the fluorescence spectrum and for temperatures ranging from 20°C to −110°C, all of the lifetime distributions obtained after MEM analysis of the decays exhibit only one short component with a negative amplitude, followed by a unique lifetime distribution. These two components are respectively attributed to "relaxational" and "emissional" lifetime distributions. Whereas the "emissional" lifetime distribution is only slightly sensitive to temperature, the "relaxational" distribution strongly depends on it. These kinetic parameters have been corrected, because these values account for the contribution of the emission decay being the harmonic mean between the emitting lifetime and the true relaxation time (Mazurenko and Bakhshiev, 1970; De Toma et al., 1976). From these corrected values, an activation energy of solvent dipolar relaxation of 3 kcal/mol was determined from the Arrhenius plot of the relaxation kinetic thermal variation. A value of 5 kcal/mol has been reported by Sagal (1962) and Bertolini et al. (1983). This discrepancy may be explained by the possible interplay between the chromophore and the relaxation process. Kinoshita and Nishi (1988) have shown, however, that the relaxation rates obtained from different dyes (rhodamine 6G, acridine red, and coumarin 7) at different temperatures were rather insensitive to the dye examined. The activation energy was similar to that reported for laurdan in the present work. The different probes used, however, can be suspected to undergo intramolecular excited-state reactions, so that the results for the solvent relaxation per se may be biased.

For short emission wavelengths and temperatures ranging from 20°C to −110°C, the lifetime distribution strongly depends on temperature. At 20°C, only one fast component with a broad distribution is deduced from the MEM analysis, whereas, as the temperature is decreased, the lifetime distribution becomes more complex. Two lifetime distributions and even three at the lowest temperatures (−110°C and −190°C) are deduced from the MEM analysis of the decays, supporting the idea that multiple excited-state reactions occur in the polar media.

The MEM analyses of the decays recorded at −190°C for blue and red emission wavelengths show a unique lifetime of ~3.7 ns preceded by two faster components. The sign of the amplitude of these two fast components depends on the emission wavelength, as expected for kinetics occurring at the excited state, but these kinetics cannot be due to solvent relaxation processes. We think that they may be related to intramolecular processes, as observed for laurdan in the apolar oils. The kinetics observed in frozen ethanol are slower than those observed in the oils. This may be due to thermal dependence of the reaction kinetics. In the model proposed in Fig. 11, we hypothesize that LE and CT excited states are responsible for the fluorescence of laurdan in apolar oils or in frozen ethanol. However, we detect only one lifetime on the decays recorded in frozen ethanol. As

the width of the lifetime distribution is large (0.7 ns), two components with similar lifetimes could be unresolved by the analysis.

The TRES experiment performed at −80°C shows that the kinetics of the excited-state stabilization is biphasic. The long relaxational time constant, which accounts for 90% of the shift, displays a value in the nanosecond range similar to that found in single decay measured in the far red edge of the fluorescence emission spectrum. It is likely related to solvent relaxation and appears to be the predominant stabilization process occurring at this temperature. The shortest relaxational component is observed in the middle range of the emission spectrum and no longer in the far red edge. According to the model presented in Fig. 11, the faster kinetics could be related to the intramolecular reaction between the LE and the CT states of laurdan that is still present in frozen ethanol. Recent observations of solvent dynamics have shown, however, that the solvent relaxation around the excited state does not obey a simple Debye relaxation time in the picosecond time range (Horng et al., 1995). This was also observed in the picosecond/nanosecond time range (Maroncelli and Fleming, 1987; Chapman et al., 1990). This short time constant could represent intramolecular motion of the ethanol molecule, like reorientation of the OH dipole.

CONCLUSION

The experiments carried out in the apolar media did show that laurdan undergoes an excited-state reaction in those solvents. This fast reaction, visualized via the red edge effect in the static experiments, but also by the time-resolved experiments, has been attributed to an intramolecular rearrangement of the probe, because the solvent cannot relax around the excited state. This fast intramolecular excited-state reaction could arise from a deformation of the molecule involving ring distortions, as described by Ilich and Prendergast (1989).

In polar media, laurdan is subjected to an important excited-state stabilization due to the solvent molecules. However, the static and dynamic results do not fit a two-state model. To account for the results in polar and apolar media, we propose a possible scheme for the deexcitation pathway (Fig. 11). Because of the heterogeneity of the absorption transitions, which has been demonstrated by the absorption spectra in both apolar and polar media, the molecule can be excited in two different states, i.e., the LE and CT states. The interconvertion between these two excited states is suggested in apolar media. Moreover, in frozen ethanol (−190°C), a composite emission spectra dependent on the excitation wavelength has been observed. The relaxation by the solvent molecules being almost impossible at this temperature, it indicates that a reaction at the excited state still exists. This reaction can therefore be attributed to the interconvertion between the excited LE and CT states, which could involve the rotation of the N-$(CH_3)_2$ group. At higher temperatures (−110 to −50°C), the emission spectra result from the radiative deexcitation of two distinct states, as indicated by the isoemissive point. These two states could be attributed to unrelaxed and relaxed charge transfer states.

The reaction pathway after the excitation in the subnanosecond and nanosecond time range can be described as involving first the planar conformation of the molecule, which is prominent in the ground state (Ilich and Prendergast, 1989). An internal charge transfer involving partial charge separation on the ring and the carbonyl group (which is strongly conjugated in the ground state, as seen by resonant Raman measurements; data not shown) can first occur, followed by twisting of the N-$(CH_3)_2$ group, which is needed to extend the charge separation on the nitrogen atom and to obtain the final CT. This highly CT state is stabilized by dipolar interactions with the solvent. This scheme accounts for almost all of the static fluorescence spectra and the kinetic data determined from fluorescence decays.

According to this scheme, the interconversion kinetics is fast compared to the lifetime of the CT state, and most of the fluorescence of the probe, in polar media, arises from the CT and CTr states. In lipidic membranes, the laurdan fluorophore is located at the interface (Chong and Wong, 1993), i.e., in a polar environment. The sensitivity of the laurdan to the gel-to-liquid crystalline phase transition could then come from modifications of the lifetimes of CT and CTr states and/or variations in the relaxation kinetics. We have shown that the lifetime of the CT state is influenced by the viscosity of the medium and that the relaxation kinetics is related to the mobility of the solvent molecules surrounding the probe and their ability to reorganize themselves around the excited state of the fluorophore. Therefore, the variation of the membrane viscosity on one hand, and of the mobility of the water molecules at the membrane interface on the other, phenomena that can be associated with the gel-to-liquid crystalline phase transition, could be responsible for the fluorescence evolution observed during the lipidic transition. The present study gives an insight into the complex deexcitation pathway of the probe and would allow a correct interpretation of the fluorescence decays of laurdan when incorporated into amphiphilic aggregates (membranes, mixed micelles). In particular, it has been shown that laurdan is very sensitive to the composition modification of the mixed octylglucoside-phosphatidylcholine micelle (Paternostre et al., 1995). In light of the present results, some qualitative and/or quantitative information may be obtained on the viscosity and the polarity of the aggregate interface as a function of their composition, size, and shape.

We acknowledge Dr. Grossiord for his valuable help in carrying out the viscosity experiments.

REFERENCES

Bagchi, B. 1989. Dynamics of solvation and charge transfer reactions in dipolar liquids. *Annu. Rev. Phys. Chem.* 40:115–141.

Balter, A., W. Nowak, W. Pawelkiewicz, and A. Kowalczyk. 1988. Some remarks on the interpretation of the spectral properties of Prodan. *Chem. Phys. Lett.* 143:565–570.

Bertolini, D., M. Cassettari, and G. J. Salvetti. 1983. The dielectric properties of alcohol-water solutions. I. The alcohol rich region. *J. Chem. Phys.* 78:365–372.

Braun, D., and W. Rettig. 1994. Kinetic studies of twisted intramolecular charge transfer in highly viscous solvents as a function of pressure and temperature. *Chem. Phys.* 180:231–238.

Buckingham, A. D. 1958. Solvent effects in infrared spectroscopy. *Proc. R. Soc. Lond.* A248:169–182.

Bunker, C. E., T. L. Bowen, and Y. Sun. 1993. A photophysical study of solvatochromic probe 9-propiony-2-(dimethylamino)naphthalene (prodan) in solution. *Photochem. Photobiol.* 58:499–505.

Chapman, C. F., R. S. Fee, and M. P. Maroncelli. 1990. Solvation dynamics in *N*-methylamides. *J. Phys. Chem.* 94:4929–4935.

Chong, P. L.-G., and P. T. T. Wong. 1993. Interactions of laurdan with phosphatidylcholine liposomes: a high pressure FTIR study. *Biochim. Biophys. Acta.* 1149:260–266.

Declémy, A., and C. Rullière. 1994. Relaxation dynamics of the solvent cage around an excited molecule in solution. *In* AIP conference proceedings 298, Ultrafast Reaction Dynamics and Solvent Effects. Y. Gauduel and P. J. Rossky, editors. American Institute of Physics, New York. 275–295.

De Toma, R., J. H. Easter, and L. Brand. 1976. Dynamic interaction od fluorescence probes with the solvent environment. *J. Am. Chem. Soc.* 98:5001–5007.

Fröhlich, H. 1958. Theory of Dielectrics. Oxford University Press.

Grabowski, Z. R., K. Rotkiewicz, A. Siemiarczuk, D. J. Cowley, and W. Baumann. 1979. Twisted intramolecular charge transfer states (TICT). A new class of excited states with full charge separation. *Nouv. J. Chim.* 3:443–454.

Heerklotz, H., H. Binder, and G. Lantzsch. 1994a. Determination of the partition coefficients of the nonionic detergent C12E7 between lipid-detergent mixed membranes and water by means of laurdan fluorescence spectroscopy. *J. Fluorescence.* 4:349–352.

Heerklotz, H., H. Binder, G. Lantzsch, and G. Klose. 1994b. Membrane water partition of oligo(ethylene oxide) dodecyl ethers and its relevance for solubilization. *Biochim. Biophys. Acta.* 1196:114–122.

Heisel, F., J. A. Miehé, and A. W. Szemik. 1987. Experimental evidence of an intramolecular reation in excited prodan solution. *Chem. Phys. Lett.* 138:321–326.

Horng, M. L., G. A. Gardecki, and M. Maroncelli. 1995. Subpicosecond measurements of polar solvation dynamics: coumarin 153 revisited. *J. Phys. Chem.* 99:17311–17337.

Ilich, P., and F. G. Prendergast. 1989. Singlet adiabatic states of solvated prodan: a semiempirical molecular orbital study. *J. Phys. Chem.* 93: 4441–4447.

Kinoshita, S., and N. Nishi. 1988. Dynamics of fluorescence of a dye molecule in solution. *J. Phys. Chem.* 89:6612–6622.

Lakowicz, J. R. 1983. Principles of Fluorescence Spectroscopy. Plenum Press, New York.

Lakowicz, J. R., and A. Balter. 1982a. Differential-wavelength deconvolution of time-resolved fluorescence intensities. A new method for the analysis of excited-state processes. *Biophys. Chem.* 16:223–240.

Lakowicz, J. R., and A. Balter. 1982b. Analysis of excited-state processes by phase modulation fluorescence spectroscopy. *Biophys. Chem.* 16: 117–132.

Livesey, A. L., and J. C. Brochon. 1987. Analyzing the distribution of decay constants in pulse-fluorimetry using the maximum entropy method. *Biophys. J.* 52:693–706.

Macgregor, R. B., and G. Weber. 1981. Fluorophores in polar media: spectral effects of the Langevin distribution of electrostatic interactions. *Ann. N.Y. Acad. Sci.* 366:140–154.

Madden, P., and D. Kivelson. 1984. A consistent molecular treatment of dielectric phenomena. *Adv. Chem. Phys.* 56:467–566.

Maroncelli, M., and G. R. Fleming. 1987. Picosecond solvation dynamics of coumarin 153: the importance of molecular aspects of solvation. *J. Chem. Phys.* 86:6221–6239.

Mazurenko, Y. T., and N. G. Bakhshiev. 1970. The influence of orientational dipolar relaxation on spectral, temporal and polarization properties of luminescence in solutions. *Optica Spectrosc. (USSR).* 28:905–913.

Merlo, S., and P. Yager. 1990. Optical method for monitoring the concentration of general anesthetics and other small organic molecules. An example of phase transition sensing. *Anal. Chem.* 62:2728–2735.

Nowak, W., P. Adamczak, and A. Balter. 1986. On the possibility of fluorescence from twisted intramolecular charge transfert states of 2-dimethylamino-6-acylnaphthalenes. A quantum-chemical study. *J. Mol. Struct. (Theochem.).* 139:13–23.

Parasassi, T., F. Conti, and E. Gratton. 1986. Time-resolved fluorescence emission spectra of laurdan in phospholipid vesicles by multifrequency phase and modulation fluorometry. *Cell. Mol. Biol.* 32:103–108.

Parasassi, T., G. De Stasio, A. d'Ubaldo, and E. Gratton. 1990. Phase fluctuation in phospholipid membranes revealed by laurdan fluorescence. *Biophys. J.* 57:1179–1186.

Parasassi, T., G. De Stasio, G. Ravagnan, R. M. Rush, and E. Gratton. 1991. Quantitation of lipid phase in phospholipid vesicles by the generalized polarization of laurdan fluorescence. *Biophys. J.* 60:179–189.

Parasassi, T., M. Di Stefano, M. Loiero, G. Ravagnan, and E. Gratton. 1994a. Cholesterol modifies water concentration and dynamics in phospholipid bilayers: a fluorescence study using laurdan probe. *Biophys. J.* 66:763–768.

Parasassi, T., M. Di Stefano, M. Loiero, G. Ravagnan, and E. Gratton. 1994b. Influence of cholesterol on phospholipid bilayers phase domains as detected by laurdan fluorescence. *Biophys. J.* 66:120–132.

Paternostre, M., O. Meyer, C. Grabielle-Madelmont, S. Lesieur, M. Ghanam, and M. Ollivon. 1995. Partition coefficient of a surfactant between aggregates and solution: application to the micelle-vesicle transition of egg-phosphatidylcholine and octyl B-D glucopyranoside. *Biophys. J.* 69:2476–2488.

Rollinson, A. M., and H. G. Drickamer. 1980. High pressure study of luminescence from intramolecular CT compounds. *J. Chem. Phys.* 73: 5981–5996.

Sagal, M. W. J. 1962. Dielectric relaxation in liquid alcohols and diols. *J. Chem. Phys.* 36:2437–2442.

Sire, O., B. Alpert, and C. A. Royer. 1996. Probing pH and pressure effects on the apomyoglobin heme pocket with the 2′-(*N,N*-dimethylamino)-6-naphthoyl-4-*trans*-cyclohexanoic acid fluorophore. *Biophys. J.* 70: 2903–2914.

Soujanya, T., R. W. Fessenden, and A. Samanta. 1996. Role of nonfluorescent twisted intramolecular charge transfer state on the photophysical behavior of aminophthalimide dyes. *J. Chem. Phys.* 100:3507–3512.

Vincent, M., J. Gallay, and A. P. Demchenko. 1995. Solvent relaxation around the excited state of indole: analysis of fluorescence lifetime distributions and time-dependence spectral shifts. *J. Phys. Chem.* 99: 14931–14941.

Wahl, P. 1979. Analysis of fluorescence anisotropy decays by a least square method. *Biophys. Chem.* 10:91–104.

Weber, G., and F. J. Farris. 1979. Synthesis and spectral properties of a hydrophobic fluorescent probe: 6-propionyl-2-(dimethylamino)naphthalene. *Biochemistry.* 18:3075–3078.